Journal of Hydrology 577 (2019) 123967

Contents lists available at ScienceDirect

Journal of Hydrology

journal homepage: www.elsevier.com/locate/jhydrol

Research papers

Applicability of Kinematic model for mud-flows: An unsteady analysis

Cristiana Di Cristo[a], Michele Iervolino[b], Tommaso Moramarco[c], Andrea Vacca[a,*]

[a] Dipartimento di Ingegneria Civile, Edile ed Ambientale, Università degli Studi di Napoli "Federico II", Via Claudio 21, 80125 Napoli, Italy
[b] Dipartimento di Ingegneria, Università degli Studi della Campania "Luigi Vanvitelli", Via Roma 29, 81031 Aversa, CE, Italy
[c] National Research Council, IRPI, Via Madonna Alta 126, Perugia, Italy

ARTICLE INFO

This manuscript was handled by Marco Borga, Editor-in-Chief

Keywords:
Mud-flow
Power-law rheology
Shear-thinning fluid
Kinematic Wave Model
Unsteady flow

ABSTRACT

The Kinematic Wave Model (KWM), representing a simplification of the Full Wave Model (FWM) under the shallow-water approximation, is often used in the one-dimensional formulation for describing the dynamics of debris/mud flood. The present work investigates the applicability conditions of the KWM to analyze mud floods, characterized by a rheological behaviour expressed through a power-law model. The study is carried out through the numerical solution of both the Full and Kinematic Wave models changing the characteristic time of hydrograph, i.e. the wave duration, imposed at the channel inlet. The predictions of the two models are compared in terms of maximum flow depth, maximum discharge and peak discharge at the downstream channel end. The study is performed for several values of the Froude (F) and the Kinematic Wave (K) numbers. Similarly to the clear-water case, present results show that higher errors in applying KWM pertain to shorter flood wave durations, but the performance of KWM appears to strongly depend on the value of the rheological index, becoming worse as the fluid rheology becomes more shear-thinning. The study furnishes applicability criteria representing a guideline for practical applications in terms of minimum wave duration above which the KWM error in reproducing the considered flood characteristics (the maximum flow depth, the maximum discharge and the peak discharge at the downstream channel end) is less or equal than 5%. Finally, it has been shown that the wave period criterion, obtained considering linearized wave dynamics, may be safely applied at least for fluid with moderate shear-thinning behavior and for moderate values of the dimensionless number KF^2.

1. Introduction

The terms debris and mud flows, used to identify rapid movement of sediment and water mixtures propagating along slopes, are classified according to a nomenclature based on the different origin, the composition and the flow characteristics (Takahashi, 2014). In particular, debris flows are characterized by the presence of gravel sediments and their dynamics is controlled by erosion, deposition and grain collisions (Gregoretti et al., 2019). Conversely, mud flows involve highly-concentrated mixtures of water and fine sediments, with a rheology strongly influenced by the quantity of the fine fraction.

Due to the modification of the rainfalls and the increased urbanization, the frequency of debris/mud flows has increased in the last decades. These phenomena have an exceptional destructive power producing severe damages on the impacted areas due to the high velocity and the large volumes of mobilized, transported and deposited sediments (Fuchs et al., 2007; Jacob et al., 2012; Thiene et al., 2017; Gregoretti et al., 2018; Stancanelli and Musumeci, 2018; Chen et al., 2019). The individuation of hazard-prone areas is of utmost importance to estimate the effect of an event on populations, properties and environment (Harms-Ringdahl, 2004; Hurlimann et al., 2006).

For individuating hazard areas, different approaches may be used based on environmental surveys and monitoring of previous events (e.g. Di et al., 2008; He et al., 2003; Hungr, 2011) and/or numerically predicting the evolution of potentially dangerous scenarios. Numerous numerical methods considering the mass, momentum and energy conservation equations have been proposed in literature for simulating the debris/mud flow propagation. A possible classification pertains to the schematization of the water-solid mixture.

A first option for the mixture analysis consists in separately describing the liquid and the solid components and therefore adopting the so-called two-phase approach (e.g. Pitman and Le, 2005; Pudasaini, 2012; He et al., 2014; Di Cristo et al., 2016). The sophisticated models proposed by Armanini et al. (2014) and by Iverson and George (2014) belong to this class, more adapt for representing debris flows in which the role of the solid and liquid phase must be distinguished. The former

* Corresponding author.
E-mail addresses: cristiana.dicristo@unina.it (C. Di Cristo), michele.iervolino@unicampania.it (M. Iervolino), tommaso.moramarco@irpi.cnr.it (T. Moramarco), vacca@unina.it (A. Vacca).

https://doi.org/10.1016/j.jhydrol.2019.123967
Received 13 February 2019; Received in revised form 15 July 2019; Accepted 17 July 2019
Available online 22 July 2019

model uses the kinetic theory for the collisional regime, dominant close to the free surface. For the frictional regime a specific model is adopted, which matches the Coulomb condition at the boundary with the loose static bed. In the model by Iverson and George (2014) the balance equations describe the coupled evolution of the solid volume fraction, the basal pore-fluid pressure, the flow thickness and the two components of flow velocity. Basal friction is evaluated using a generalized Coulomb rule, and the fluid motion is evaluated in a reference frame that translates with the velocity of the granular phase. Source terms in each of the depth-averaged balance equations account for the influence of the granular dilation rate, considering both the effects of elastic compressibility and of an inelastic dilatancy angle.

A different approach models the mixture as a homogeneous single-phase medium with a non-Newtonian behaviour (Takahashi, 2014). The characteristics of the apparent fluid are defined by the relationship between the shear stress and the strain rate that is called the constitutive law. The most commonly used single phase models are: Bingham (yielding with subsequent Newtonian behaviour), power-law or Ostwald–de Waele, Herschel-Bulkley (yielding with subsequent power-law behaviour). Moreover, it is often adopted also a variant of the Bingham model which introduces a quadratic term, aiming to account even for the turbulent/dispersive terms (O'Brien et al., 1993). The models with a yield stress, often called visco-plastic, reproduce the stopping of the flow as a deposit in flat areas and they are therefore widely used in many engineering applications (e.g. Coussot, 1997; Huang and Garcia, 1998; Chanson et al., 2006; Ancey, 2007; Chambon et al., 2009; Pastor et al., 2014). However, since a correct rheology characterization of the visco-plastic fluids is a subtle task (Ovarlez et al., 2011; Chambon et al., 2014), also the power-law (without yield stress) rheology is often employed (e.g. Jeong et al., 2009).

Values of the power-law exponent larger than one refer to dilatant (or shear-thickening) fluids, while values smaller than one describe the shear-thinning behavior. The widely used Bagnold rheology belongs to the former category (the exponent is equal to two) and it is employed for representing stony-type debris flow in which the grain-collisions are dominant (Pudasaini, 2011; Takahashi, 2014). Conversely, the shear-thinning power-law model is particularly adequate for describing fine magmas and mining residuals, dilute clay or kaolin suspensions, and river flows with a finite fraction of coarse grains, such as mud-flows (Ng and Mei, 1994; Hwang et al., 1994; Perazzo and Gratton, 2004; Longo et al., 2015). For instance, shear-thinning power-law model has been found to mimic the rheology of both the natural estuarine mud dredged from Haihe River in Tianjin and Mazhou Island (Zhang et al., 2010) and the catastrophic landslide occurred in 1999 in Cervinara, Italy (Carotenuto et al., 2015).

Starting from the Cauchy momentum equations and assuming a power-law relation between the stress and the rate of strain tensors, several shallow-layer models have been proposed. Owing to its simplicity, the model deduced through the von Kàrmàn momentum integral method, i.e. Saint-Venant equations, is often preferred in environmental applications to other more rigorous models such as the ones deduced through either the asymptotic expansions of the solution of the Cauchy momentum equations (e.g. Fernández-Nieto et al., 2010; Noble and Vila, 2013) or the weighted residual method (e.g. Ruyer-Quil and Manneville, 2002).

Independently on the approach used for describing the solid-liquid mixture, i.e. two- or single- phase, the two-dimensional shallow-layer models allow to accurately reproduce the mud-flow dynamics (Armanini et al., 2009, 2014; Di Cristo et al., 2018; Fent et al., 2018; Greco et al., 2019; Iverson and George, 2014; Medina et al., 2008; O'Brien et al., 1993; Rosatti and Begnudelli, 2013) but they require considerable computational time and storage. Moreover, their application is particularly challenging in presence of irregular topography (Yan et al., 2013). These limitations prevent their use for large scale investigations and for civil protection studies where quick analyses of the possible impacted areas are required. To overcome such a constraint, simplified models are often employed for describing the dynamics of debris/mud flows (e.g. O'Brien et al., 1993; Arattano and Savage, 1994; Chiang et al., 2012; Deangeli, 2008; Gregoretti et al., 2016, 2019; Bernard et al., 2019). Simplified models are less computationally expensive than the full one and they are also characterized by a less sensitive response to the noise in the input data (Yu and Lane, 2006; Weill et al., 2014; Aricò et al., 2016). In this context is of utmost importance to define the conditions in which the simplified models can be used with enough accuracy.

The Kinematic Wave Model, neglecting in the momentum equation the local and convective inertia and the pressure gradient terms, is the simplest approximation. A direct comparison between the results of the Kinematic model with experimental data has been carried out by Arattano et al. (2006), with reference to the debris flow occurred in 2004 in an experimental basin on the Italian Alps. The rheological model is characterized by the presence of a yield stress plus a quadratic term (Honda and Egashira, 1997). It has been shown that the simplified model is able to describe the main features of the flood. Moreover, the comparison with of the full model led the authors to conclude that the rheological parameters influence the results more than the inertial terms in the Saint-Venant equations, giving additional support to the use of the Kinematic Wave Model for the debris flow prediction. Unfortunately, as far as shear-thinning fluids are concerned, a similar comparison between the outcomes of the Kinematic Wave Model with field data is not available. However, for this kind of fluids, the validity of the kinematic approximation has been tested by Longo et al. (2015) in reproducing laboratory dam-break tests performed in a constant slope channel with different cross-sections. A good agreement between the experiments and the theoretical developments, in terms of front position, has been observed particularly at late times. In the early stage, the discrepancies were attributed to the high depth-to-length aspect ratio. The above analysis has been extended to the case of a varying longitudinal channel slope in Longo et al. (2016), confirming the validity of the simplified model.

Even if applicability criteria of simplified models have been widely studied for flood of clear-water, (e.g. Ponce et al., 1978; Moussa and Boequillon, 1996; Singh and Aravamuthan, 1996; Tsai, 2003; Perumal and Sahoo, 2007; Moramarco et al., 2008a,b), only few works addressed the problem for non-Newtonian fluids. With reference to a power-law rheology, Di Cristo et al., (2014) deduced the applicability criteria of some approximated models (i.e. kinematic, diffusion and quasi-steady) in terms of dimensionless wave period of the flow perturbation. Assuming as initial condition the uniform one, the linearized version of both the full and the approximated models in an unbounded channel has been analyzed. The study has been extended to finite-length channels in Di Cristo et al. (2018b) through the evaluation of the upstream and downstream channel response functions of the linearized problem. Recently, Di Cristo et al., 2018c have investigated the applicability conditions of the kinematic and the diffusive wave models in power-law flows, accounting for the non-linearity of governing equations. The study compared the analytical solution of the steady flow depth profiles predicted by the approximated models with those of the full dynamic wave one in a channel of finite length. The results put in evidence the important effect of the rheology, revealing also that the applicability ranges of both approximated models may strongly differ from the corresponding ones for the clear-water case.

The present paper aims to extend to unsteady flow conditions the previous study of Di Cristo et al., 2018c by investigating the applicability of the simplified Kinematic Wave Model (KWM) in predicting the propagation of a mud-flow. This work considers the power-law model proposed by Ng and Mei (1994) for reproducing mud-flows characterized by a highly-concentrated mixture of water and fine sediments, which usually occur in river flows with a small fraction of coarse grains. The model is deduced through the von Karman momentum integral method and accounts for the variation of the velocity distribution along the flow depth.

In this context, the accuracy of the KWM in reproducing some characteristics of mud-floods with a power-law rheology is analyzed. The study is carried out through a numerical analysis of both the Full and the Kinematic Wave models considering at the channel inlet discharge hydrographs characterized by different wave periods. An explicit first-order scheme for the temporal discretization and a second-order Finite-Volume method for the spatial discretization are used. The applicability conditions are expressed considering three dimensionless parameters, related to the error on the maximum flow depth, the maximum discharge and the peak discharge at the downstream end of the channel. The effect of the rheology on the KWM applicability is deeply investigated and the derived criteria are compared with the analytical ones obtained by Di Cristo et al. (2014).

The paper is organized as follows. Section 2 reports the governing equations for the Full Wave Model (FWM) and of the Kinematic Wave Model (KWM), while in Section 3 the numerical methods are presented. Section 4 illustrates the results of the comparison between the FWM and the KWM and the obtained applicability criteria. Finally, conclusions are drawn in Section 5.

2. Governing equations

Let us consider a one-dimensional unsteady, gradually-varied, laminar flow of a layer of power-law fluid flowing over a non-erodible bed, inclined of an angle θ with respect to the horizontal plane. Lateral inflow or outflow are not allowed. The dimensional depth-averaged momentum and mass conservation equations are (Di Cristo et al., 2013a):

$$\frac{\partial \widetilde{q}}{\partial \widetilde{t}} + \beta \frac{\partial}{\partial \widetilde{x}}\left(\frac{\widetilde{q}^2}{\widetilde{h}}\right) + g\widetilde{h}\frac{\partial \widetilde{h}}{\partial \widetilde{x}}\cos\theta = g\widetilde{h}\sin\theta - \frac{\widetilde{\tau}_b}{\rho} \tag{1}$$

$$\frac{\partial \widetilde{h}}{\partial \widetilde{t}} + \frac{\partial \widetilde{q}}{\partial \widetilde{x}} = 0 \tag{2}$$

where $\widetilde{t}$ is the time, $\widetilde{x}$ is the streamwise coordinate, $\widetilde{h}$ the flow depth, $\widetilde{q}$ the flow rate (for unit of width), g and ρ the gravity and the fluid density, respectively. β and $\widetilde{\tau}_b$ are the momentum correction factor and the bottom stress, respectively.

Denoting with $\widetilde{u} = \widetilde{q}/\widetilde{h}$ the depth averaged velocity, in laminar regime the expressions of the momentum correction factor and of the bottom stress are (Di Cristo et al., 2013; Ng and Mei, 1994), respectively:

$$\beta = 2\frac{2n+1}{3n+2} > 1 \tag{3}$$

$$\widetilde{\tau}_b = \mu_n\left(\frac{2n+1}{n}\frac{\widetilde{u}}{\widetilde{h}}\right)^n \tag{4}$$

μ_n and n being the consistency and the rheological index of the power law fluid, respectively.

If the rheological index n is smaller than one (shear-thinning fluid), the effective viscosity decreases with the deformation amount, modelling the disintegration of fluid structure under shear. Conversely, when the rheological index is larger than one (shear-thickening fluids), the viscosity increases with the amount of shearing, implying that the fluid microstructure is build up by the fluid motion (Mei et al., 2001). In this work, only shear- thinning fluids have been considered.

Denoting with $\widetilde{L}$ the dimensional channel length, for a given flow rate $\widetilde{q}_{ref}$ (for unit width), the following dimensionless quantities are introduced:

$$x = \widetilde{x}/\widetilde{L} \quad t = \widetilde{t}\,\widetilde{q}_{ref}/(\widetilde{L}\widetilde{h}_N) \quad h = \widetilde{h}/\widetilde{h}_N \quad q = \widetilde{q}/\widetilde{q}_{ref} \tag{5}$$

where $\widetilde{h}_N$ denotes the dimensional normal, i.e. uniform, flow depth corresponding to $\widetilde{q}_{ref}$ Accounting for Eq. (5) and (3), Eqs. (1) and (2) may be rewritten in their dimensionless form as follows:

$$\frac{\partial h}{\partial t} + \frac{\partial q}{\partial x} = 0 \tag{6}$$

$$\frac{\partial q}{\partial t} + \frac{\partial}{\partial x}\left(\beta\frac{q^2}{h}\right) + \frac{\partial}{\partial x}\left(\frac{h^2}{2F^2}\right) = Kh\left(1 - \frac{q^n}{h^{2n+1}}\right) \tag{7}$$

where the normal Froude number, F, and the kinematic wave number, K, are:

$$F = \frac{\widetilde{q}_{ref}}{\widetilde{h}_N^{3/2}\sqrt{g\cos\theta}}, \quad K = \frac{1}{F^2}\frac{\widetilde{L}}{\widetilde{h}_N}\tan\theta \tag{8}$$

Similarly to the Turbulent Clear Water (TCW) case (Govindaraju et al., 1988a,b; Moramarco et al., 2008a) even for the power-law fluids, the two dimensionless numbers F and K uniquely define the problem under investigation. In what follows, similarly to the TCW case (Moramarco et al., 2008a) one of the two pairs (F, K) or (F, KF^2) is considered.

It is easy to verify that the system (6)–(7) is hyperbolic and the expression of the characteristic slopes is (Di Cristo et al., 2017):

$$\lambda_{\pm} = \beta\frac{q}{h} \pm \sqrt{\beta(\beta-1)\frac{q^2}{h^2} + \frac{h}{F^2}} \tag{9}$$

The KWM is obtained neglecting in the momentum equation the local and convective inertia and the pressure gradient terms, represented by all terms at the l.h.s. of Eq. (7). Therefore, starting from the simplified version of Eq. (7), the flow rate may be expressed only in terms of flow depth $\left(q(h) = h^{2n+1/n}\right)$ and by substituting this expression in Eq. (6) the following equation is deduced:

$$\frac{\partial h}{\partial t} + \frac{\partial}{\partial x}\left(h^{\frac{2n+1}{n}}\right) = 0 \tag{10}$$

Conversely, expressing the flow depth only in terms of flow rate $\left(h(q) = q^{n/2n+1}\right)$ and rewriting Eq. (6) as follows:

$$\frac{\partial q}{\partial t} + \frac{\mathrm{d}q}{\mathrm{d}h}\frac{\partial q}{\partial x} = 0 \tag{11}$$

the following version of KWM in terms of flow rate only is obtained:

$$\frac{\partial q}{\partial t} + \frac{\partial}{\partial x}\left[\frac{(2n+1)^2}{n(3n+2)}q^{\frac{3n+2}{2n+1}}\right] = 0 \tag{12}$$

The linearized version, around the reference state, of Eqs. (10) or (12) allows to easily deduce the following expression for dimensionless celerity of the KWM:

$$c_{KWM}^{PLF} = \frac{2n+1}{n} \tag{13}$$

in agreement with the findings of Di Cristo et al. (2014). While in for Turbulent Clear Water flows the celerity of the KWM is constant and equal to 3/2, Eq. (13) indicates that for a power-law fluid it depends on the rheological index.

3. Unsteady analysis

3.1. Numerical solution of Full Wave Model

The numerical solution of system (6)–(8) is pursued by using an explicit first-order scheme for the temporal discretization and a second-order Finite-Volume method for the spatial discretization. Rewriting Eqs. (6)–(7) in the following compact form:

$$\frac{\partial \mathbf{w}}{\partial t} + \frac{\partial \mathbf{F}(\mathbf{w})}{\partial x} = \mathbf{s}(\mathbf{w}) \tag{14}$$

where:

$$\mathbf{w} = \begin{bmatrix} h \\ q \end{bmatrix}, \quad \mathbf{F}(\mathbf{w}) = \begin{bmatrix} q \\ \beta\frac{q^2}{h} + \frac{1}{2}\frac{h^2}{F^2} \end{bmatrix}, \quad \mathbf{s}(\mathbf{w}) = \begin{bmatrix} 0 \\ K\frac{h^{2n+1} - q^n}{h^{2n}} \end{bmatrix} \tag{15}$$

the corresponding discretized equation reads

$$\frac{\bar{\mathbf{w}}_i^{k+1} - \bar{\mathbf{w}}_i^k}{\Delta t} + \frac{1}{\Delta x}(\hat{\mathbf{F}}_{i+1/2}^k - \hat{\mathbf{F}}_{i-1/2}^k) = \bar{\mathbf{s}}_i^k \tag{16}$$

in which $\bar{\mathbf{w}}_i$ and $\bar{\mathbf{s}}_i$ are the averaged values of the variable $\mathbf{w}$ and of the source term (pointwisely evaluated) $\mathbf{s}$ in the i-th volume. In Eq. (16) the k superscript refers to time $t^k = k\Delta t$, with Δt the integration time step and Δx the finite volume length, while $\hat{\mathbf{F}}_{i-1/2}$ and $\hat{\mathbf{F}}_{i+1/2}$ represent the numerical approximation of the fluxes at the volume interfaces $i - 1/2$ and $i + 1/2$, respectively. The following expression of $\hat{\mathbf{F}}$ is considered (Harten et al., 1983):

$$\hat{\mathbf{F}} = \begin{cases} \mathbf{F}^L & \text{if } 0 \leqslant \lambda^L \\ \frac{\lambda^R\mathbf{F}^L - \lambda^L\mathbf{F}^R + \lambda^R\lambda^L(\mathbf{w}^R - \mathbf{w}^L)}{\lambda^R - \lambda^L} & \text{if } \lambda^R \leqslant 0 \leqslant \lambda^L \\ \mathbf{F}^R & \text{if } 0 \geqslant \lambda^R \end{cases} \tag{17}$$

with:

$$\lambda^R = \max_{R,L}(\lambda_+, 0), \quad \lambda^L = \min_{R,L}(\lambda_-, 0) \tag{18}$$

In Eq. (17) $\mathbf{w}^L$ and $\mathbf{w}^R$ represent a piecewise linear reconstruction of $\mathbf{w}$ on the left and right sides of the volume interface, respectively. In order to preserve the monotonicity of the scheme, in the reconstruction process the min-mod operator (Gottlieb and Shu, 1998) is applied. Additional details on the numerical model may be found in Di Cristo et al. (2017).

3.2. Numerical solution of Kinematic Wave model

The KWM is solved in terms of flow rate variable q through Eq. (12) rewritten as follows:

$$\frac{\partial q}{\partial t} + \frac{\partial f(q)}{\partial x} = 0 \quad \text{with } f(q) = \frac{(2n+1)^2}{n(3n+2)}q^{\frac{3n+2}{2n+1}} \tag{19}$$

Eq. (19) is numerically integrated again through an explicit first-order scheme in time and a second-order Finite-Volume scheme in space applying the Euler- MUSCL-Hancock method (Toro, 2009). The discretized version reads:

$$\frac{\bar{q}_i^{k+1} - \bar{q}_i^k}{\Delta t} + \frac{1}{\Delta x}(\hat{f}_{i+1/2}^k - \hat{f}_{i-1/2}^k) = 0 \tag{20}$$

where $\bar{q}_i^k$ is the flow rate averaged value in the i-th volume at the time t^k. In Eq. (20) $\hat{f}_{i+1/2}^k$ and $\hat{f}_{i-1/2}^k$ represent the numerical approximation of the fluxes at the volume interfaces $i + 1/2$ and $i - 1/2$, respectively, and they read (Toro, 2009):

$$\hat{f}_{i+1/2}^k = f\left(\bar{q}_i^k + \frac{1}{2}(1 - CFL_i)\Delta q_{i+1/2}\Delta x\right),$$
$$\hat{f}_{i-1/2}^k = f\left(\bar{q}_{i-1}^k + \frac{1}{2}(1 - CFL_i)\Delta q_{i-1/2}\Delta x\right) \tag{21}$$

where $\Delta q_{i+1/2}$ (resp. $\Delta q_{i\text{-}1/2}$) is the slope of $q(x)$ function at the $i + 1/2$ (resp. i-1/2) interface and the CFL_i number is evaluated in the i-th volume at the time t^k as:

$$CFL_i = \frac{2n+1}{n}(\bar{q}_i^k)^{\frac{n+1}{2n+1}}\frac{\Delta t}{\Delta x} \tag{22}$$

In order to preserve the scheme monotony, the Superbee limiter (Toro, 2009) has been applied in calculating both slopes $\Delta q_{i+1/2}$ and $\Delta q_{i\text{-}1/2}$.

3.3. The performed tests

Following Moramarco et al. (2008b), in the present study several tests considering different flow conditions, characterized by different synthetic hydrographs imposed at the channel inlet, have been carried out. Each hydrograph is characterized by a wave duration $T = mT_0'$, with T_0' the dimensionless time to peak and m an integer larger than 1. The dimensionless time to peak T_0' is evaluated as the wave travel time of the reference flow rate and therefore, accounting for the reference length scale, it reads:

$$T_0' = \frac{1}{c_{KWM}^{PLF}} = \frac{n}{2n+1} \tag{23}$$

As indicated in Eq. (23), T_0' is only function of the fluid rheology. The following four-parameters Pearson type III distribution is assumed for the hydrograph shape (Moramarco et al., 2008b):

$$q(0, t) = q_p\left(\frac{t}{T_0'}\right)^{\frac{1}{\gamma-1}} e^{\left(\frac{1-\frac{t}{T_0'}}{\gamma-1}\right)} \tag{24}$$

where q_p is the dimensionless peak discharge and γ is the shape dimensionless factor, which assumes two different values for the rising ($\gamma = \gamma_{ris}$ for $t < T_0'$) and the recession ($\gamma = \gamma_{rec}$ for $t > T_0'$) limbs, respectively. For all tests, q_p is assumed equal to 2 and γ_{ris} equal to 1.3, according to Moramarco et al. (2008b). Then, the γ_{rec} value is defined imposing as condition that the time-averaged value of the discharge equals the dimensionless reference discharge ($q_{ref} = 1$), expressed as:

$$\frac{1}{T}\int_0^T q(0, t)dt = 1 \tag{25}$$

In the performed tests it results that the γ_{rec} value ranges between 1.1 and 51 for m between 2 and 90.

Idealized input hydrographs are often used in numerical tests for flood routing (e.g. Perumal and Sahoo 2007; Perumal et al. 2007; Moramarco et al. 2008b; Dottori et al. 2009; Fenton 2019). Moreover, Zucco et al. (2015) showed that the adopted hydrograph shape, after calibration, well lends itself to represent also the actual single-peak floods occurring in natural channels. Considering the correlation between debris/mud-flow discharge and water flow discharge (Takahashi 1991; VanDine 1985; Chen et al. 2008), the hydrograph shape adopted for the numerical tests may be considered also representative for debris/mud flows.

For the KWM none additional boundary condition is required. For the FDM whenever at the channel inlet the current is hypercritical, i.e. λ_- assumes positive value, an additional boundary condition has to be assigned. Imposing the validity of rating curve, at each time, the following flow depth value at the channel inlet is prescribed:

$$h(0, t) = q(0, t)^{n/(2n+1)} \tag{26}$$

Following Moramarco et al. (2008b), in hypocritical condition the critical flow depth is imposed as boundary condition at the channel outlet, which for a power-law fluid reads (Di Cristo et al., 2018c):

$$h(1, t) = \sqrt[3]{\beta q^2(1, t)F^2} \tag{27}$$

Several tests have been carried out with the following values of the wave period T = 2 T_0', 3 T_0', …, 10 T_0', 20 T_0', 30 T_0', 60 T_0', 90 T_0'. The Froude number have been fixed in the ranges and 0.5–0.8 and the dimensionless parameter KF^2 has been varied up to 20. As far as the rheology of the fluid is concerned, the whole shear-thinning range has been explored, namely $n \leq 1$.

All simulations have been performed with fixed values of Δx and Δt, namely $\Delta x = 0.005$ and $\Delta t = 10^{-6}$ verifying that the Courant condition has been always satisfied.

4. Results

4.1. Unsteady analysis results

The accuracy of the KWM in reproducing the results of the FWM is assessed using different dimensionless indicators (Moramarco et al., 2008b). Firstly, the dimensionless error on the maximum flow depth, $\varepsilon_{h\,\max}$, and the maximum discharge, $\varepsilon_{q\,\max}$, along the channel are evaluated as:

$$\varepsilon_{h\,\max}(x) = \frac{h_{\max}^{KWM}(x) - h_{\max}^{FWM}(x)}{h_{\max}^{FWM}(x)} 100 \tag{28}$$

$$\varepsilon_{q\,\max}(x) = \frac{q_{\max}^{KWM}(x) - q_{\max}^{FWM}(x)}{q_{\max}^{FWM}(x)} 100 \tag{29}$$

In Eq. (28) (respectively Eq. (29)) $h_{\max}^{FWM}$ and $h_{\max}^{KWM}$ (respectively $q_{\max}^{FWM}$ and $q_{\max}^{KWM}$) are the dimensionless maximum flow depth (respectively discharge) computed by the FWM and the KWM, respectively. Secondly, the mean values of $\varepsilon_{h\,\max}$and $\varepsilon_{q\,\max}$ along the channel, namely $\varepsilon_{h\,\max}^{*}$ and $\varepsilon_{q\,\max}^{*}$, are considered. With the aim of excluding the regions where the boundary conditions may have a large influence, $\varepsilon_{h\,\max}^{*}$ and $\varepsilon_{q\,\max}^{*}$ are computed limitedly for $0.05 \le x \le 0.95$ (Moramarco et al., 2008b). Finally, a third index is considered, namely the percent error of the peak discharge at the outlet, defined as:

$$\varepsilon_{Qp} = \left(\frac{Q_p^{KWM}}{Q_p^{FWM}} - 1\right) 100 \tag{30}$$

being Q_p^{FWM} and Q_p^{KWM} the peak discharge at the outlet computed by the FWM and the KWM, respectively.

Fig. 1a,b represent the effect of the rheology on the maximum flow depth error $\varepsilon_{h\,\max}$ along the channel, considering, for the sake of example, $KF^2 = 7.5$ and $F = 0.5$. Two different fluids, characterized by $n = 0.25$ and $n = 1$, are considered. Each curve refers to a single wave duration ranging between $2\,T_0'$ and $90\,T_0'$. The maximum flow depth error $\varepsilon_{h\,\max}$ varies along the abscissa and it depends on both the rheological index and the wave duration. For both n values and similarly to the turbulent clear-water case (Moramarco et al., 2008b), all curves show a monotone behavior with respect to both the channel abscissa, with an increase of $\varepsilon_{h\,\max}$ in the downstream direction. Moreover, the maximum flow depth error $\varepsilon_{h\,\max}$ decreases with the wave duration, with errors lower than 10% for $T/T_0' < 30$ for both considered rheologies. Finally, the rheology substantially affects the magnitude of the errors (Fig. 1a,b): highest errors are observed for the smallest rheological index. For instance, for $T/T_0' = 2$, at $x = 0.3$ the error is 36% for $n = 0.25$, while decreases to 7% for $n = 1.0$. Independently of the T/T_0' value, for $n = 1.0$ the error is less than 5% for $x \le 0.26$ while for $n = 0.25$ such a bound for the error is overwhelmed in the whole channel for $T/T_0' < 20$. A more extensive analysis performed considering different combinations of the pair (F, KF^2) values (results not shown) confirms the qualitative results observed in Fig. 1.

To better assess the effect of the rheology on the applicability conditions, Fig. 2a,b report in the (x, KF^2) plane, for $F = 0.5$ and for four different rheological indexes ($n = 0.25, 0.50, 0.75, 1.0$), the region where the KWM is applicable with an error less than 5% based on the $\varepsilon_{h\,\max}$ indicator. Two different wave durations have been considered, namely $T/T_0' = 2$ (Fig. 2a) and $T/T_0' = 20$ (Fig. 2b). For a fixed n value, the region of the (x-KF^2) plane to the left of the curve corresponds to the conditions of local applicability of the approximated model. Fig. 2c,d are the counterparts of Fig. 2a,b with $F = 0.8$.

For a fixed n value and independently of the Froude number value and the wave duration, all plots of Fig. 2 suggest that the applicability region enlarges with the KF^2 values, similarly to the turbulent clear-water case (Moramarco et al., 2008b). Moreover, for a given triplet (KF^2, F, T/T_0'), the performance of the approximated model deteriorates as the fluid rheology becomes more shear-thinning, i.e. when n reduces. For instance, considering $KF^2 = 10$ at $F = 0.5$ and $T/T_0' = 2$, Fig. 2a indicates that the KWM predicts with the prescribed tolerance the maximum flow depth in about the first 30% of the channel length for $n = 1$, while this length becomes less than 10% in the $n = 0.25$ case. For a concise comparison, Table 1 reports the upper bounds of the channel abscissa (x_{lim}) for the applicability of the KWM at $KF^2 = 10$ for the different rheological indexes.

The values reported in Table 1, compared with the one pertaining to the turbulent clear-water case $x_{lim}^{TCW} \sim 0.5$ (see Fig. 2 of Moramarco et al., 2008b), allow to conclude that the laminar power-law rheology strongly reduces the applicability conditions of the KWM.

The combined examination of Fig. 2a,c, corresponding to the same wave duration ($T/T_0' = 2$), but referring to different Froude numbers, suggests that the Froude number value has a negligible influence on the performance of the KWM. Some small differences are observed only for small KF^2 values and for fluids with a small rheological index. The same comparison for the higher wave duration, $T/T_0' = 20$ (Fig. 2b and d), shows differences with a larger applicability region for the lower Froude number ($F = 0.5$), with increasing differences for lower rheological index values. For instance, in the case $F = 0.5$ for $n = 0.25$ and $KF^2 = 10$ the KWM is applicable in the first 85% of the channel, while for $F = 0.8$ it reduces to the 65%.

The enlargement of the applicability region with KF^2 (for a fixed value of F) may be easily explained by inspecting the dimensionless momentum conservation equation (Eq. (7)). For large values of KF^2, for a fixed value of the Froude number, the r.h.s., of Eq. (7) becomes the leading term and therefore the FWM tends to the Kinematic one. The effect of the wave duration on the applicability of KWM may be again theoretically explained based on the dimensionless momentum equation. Indeed, an increase of the wave duration reduces the l.h.s. of Eq. (7) reducing the local inertia term.

Previous results demonstrate that the KWM accurately

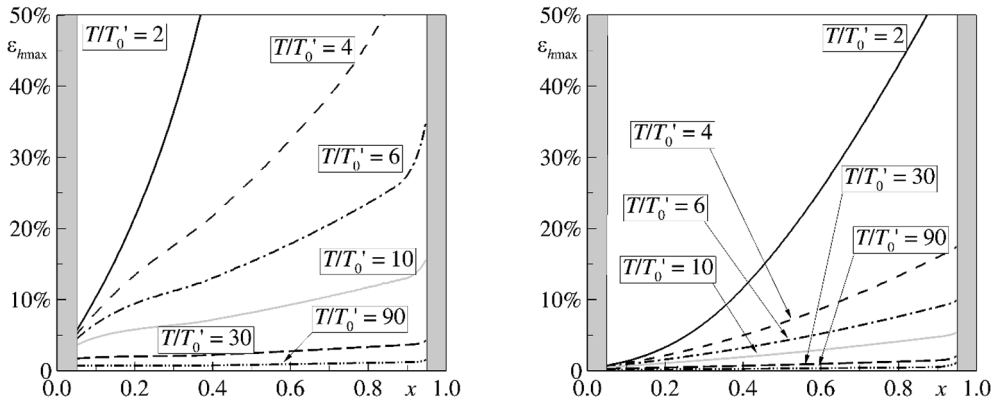

Fig. 1. Error on the maximum flow depth $\varepsilon_{h\,\max}$ along the channel for several values of the T/T_0' ratio. $KF^2 = 7.5$ and $F = 0.5$. a) $n = 0.25$. b) $n = 1.0$.

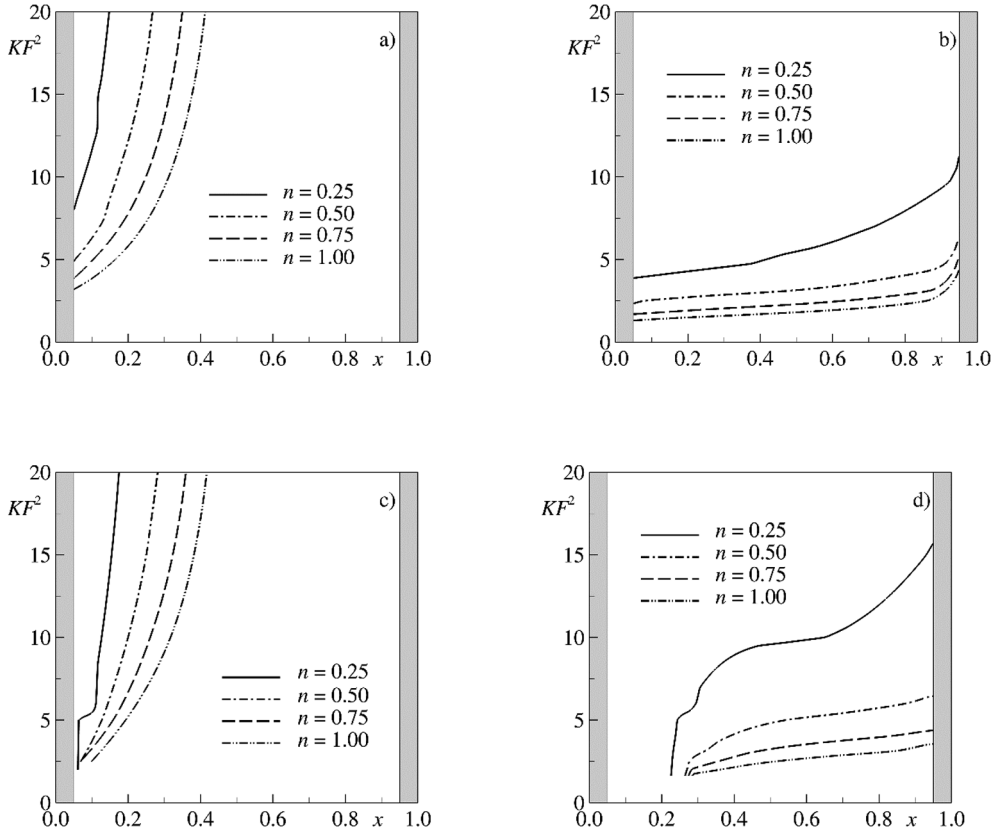

Fig. 2. Applicability Region of the KWM for four different rheological indexes (n = 0.25, 0.5, 0.75, 1.0) in the (x, KF^2) plane considering $\varepsilon_{h\,\max}$ less than 5% a) $T/T_0' = 2$ and $F = 0.5$; b) $T/T_0' = 20$ and $F = 0.5$; c) $T/T_0' = 2$ and $F = 0.8$; d) $T/T_0' = 20$ and $F = 0.8$.

Table 1
Channel abscissa upper bound (x_{lim}) for $\varepsilon_{h\,\max}$ less than 5% for the different rheological indexes. ($T/T_0' = 2$, $F = 0.5$, $KF^2 = 10$).

n	0.25	0.50	0.75	1.00
x_{lim}	0.07	0.16	0.24	0.31

approximates FDM over the entire channel length, i.e. $\varepsilon_{h\,\max} < 0.05$ for $0 < x < 1$ only for sufficiently large values of T/T_0'. A less restrictive criterion may be derived considering the mean error of the maximum flow depth $\varepsilon^*_{h\,\max}$. For $F = 0.5$, Fig. 3 reports $\varepsilon^*_{h\,\max}$ as function of the wave duration for the same rheological indexes of Fig. 2 and two different KF^2 values, namely $KF^2 = 2.5$ (Fig. 3a) and $KF^2 = 20$ (Fig. 3b).

Coherently with Figs. 1 and 2, in all cases the mean error $\varepsilon^*_{h\,\max}$ decreases with $T/T_0'$and it is affected by KF^2. Similarly to TCW (Moramarco et al., 2008b), $\varepsilon^*_{h\,\max}$ decreases when KF^2 increases. The comparison among the different curves confirms the strong dependence of the error on the rheology, with a reduction of $\varepsilon^*_{h\,\max}$ for increasing n. For instance, for $KF^2 = 2.5$ (Fig. 3a), the mean error is less than 5% for $T/T_0' > 45$ and $T/T_0' > 16$ for $n = 0.25$ and $n = 1.0$, respectively. In this way, it is possible to individuate the minimum value of T/T_0' above which the KWM can be applied with the prescribed accuracy.

For $F = 0.5$ Fig. 4 depicts $\varepsilon^*_{q\,\max}$ as function of the wave duration for $KF^2 = 2.5$ (Fig. 5a) and $KF^2 = 20$ (Fig. 5b) for different rheological indexes.

Similarly to $\varepsilon^*_{h\,\max}$, the mean error on the maximum discharge has a monotone reduction with $T/T_0'$and it decreases with KF^2. Comparing Figs. 3 and 4, it is evident that the mean error on the maximum discharge is higher than $\varepsilon^*_{h\,\max}$, while the dependency from the rheology is

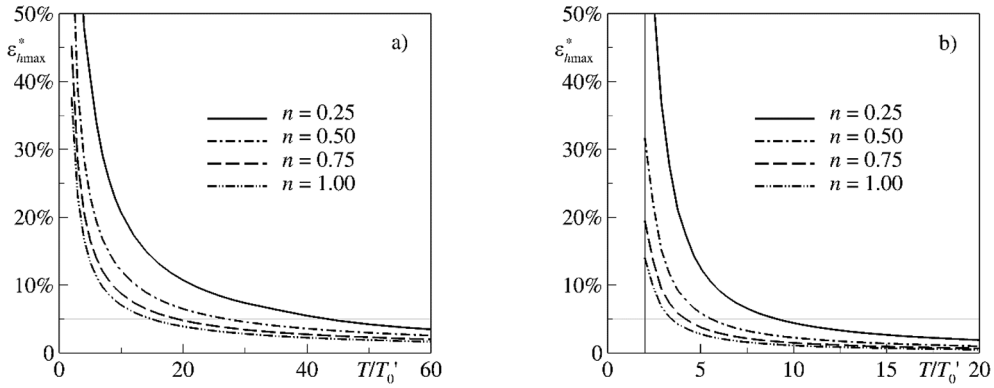

Fig. 3. Mean error of the maximum flow depth $\varepsilon^*_{h\,\max}$ as function of the ratio between the wave period and the wave reference travel time for different rheological indexes (n = 0.25, 0.50, 0.75, 1.0). $F = 0.5$. a) $KF^2 = 2.5$; b) $KF^2 = 20$.

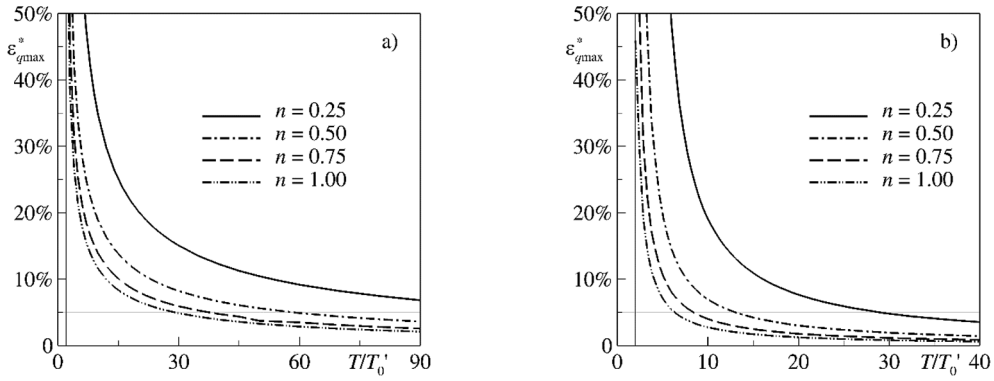

Fig. 4. Mean error on the maximum discharge $\varepsilon^*_{q\max}$ as function of the ratio between the wave period and the wave reference travel time for different rheological indexes (n = 0.25, 0.50, 0.75, 1.0). F = 0.5. a) KF^2 = 2.5b) KF^2 = 20.

similar. For instance, for KF^2 = 2.5 (Fig. 4a), $\varepsilon^*_{q\max}$ is always larger than 5% for n = 0.25, while for n = 1.0 it is less than 5% for $T/T_0' > 30$. Present results suggest that the minimum value of T/T_0' individuated for $\varepsilon^*_{h\max}$ does not provide the same accuracy in terms of mean error on the maximum flow discharge.

Fig. 5 is the counterpart of Figs. 3 and 4 in terms of error of the peak discharge at the outlet. ε_{Qp} has the same behavior of the other two considered indicators with respect to T/T_0' and KF^2, but it has larger values than both $\varepsilon^*_{h\max}$ and $\varepsilon^*_{q\max}$. In fact, for KF^2 = 2.5 (Fig. 5a), ε_{Qp} for the cases n = 0.25 and n = 0.5 is always larger than 5%.

For all the considered parameters, the results obtained with F = 0.8 (not reported herein) are very similar, with some differences only for the smallest rheological index value and for wave durations $T/T_0' < 20$. These observations confirm a larger influence of KF^2 and a minor effect of the Froude value on the KWM applicability condition.

In conclusion, the range of conditions in which the KWM has a mean error of the maximum flow depth less than 5% is wider than the one necessary for obtaining the same accuracy in terms of maximum flow discharge and peak discharge at the outlet. The rheological characterization is crucial, because for small n values in many cases the KWM is not able to reproduce the FDM solutions with an accuracy above 95%. Finally, the results shown in Figs. 2–5 allow to define the applicability conditions of the KWM and they can be used as a guideline for practical applications.

4.2. Comparison with the wave period criterion

In what follows, the results of the performed numerical analysis are employed to assess the effectiveness of the theoretical criterion proposed by Di Cristo et al. (2014), which generalizes to power-law fluids the wave period criterion proposed by Ponce et al. (1978) for clear-water flood routing. Similarly to Ponce et al. (1978), the criterion of Di Cristo et al. (2014) provides a lower bound of the dimensionless wave period (Θ) above which the KWM approximates the FDM within a prescribed accuracy. It is worth of nothing that the wave period criteria are applicable only to linearly stable flow conditions. Therefore, as far as power law fluids are concerned, the criterion of Di Cristo et al. (2014) holds only for $F < F^*$, F^* being the limiting linear stability Froude number (Ng and Mei, 1994):

$$F^* = \frac{n}{\sqrt{2n+1}} \tag{31}$$

In order to verify the wave period criteria for clear-water flood routing, Moramarco et al. (2008a) related the dimensionless wave period Θ to the wave duration (T/T_0') through the following relation:

$$\Theta = \frac{KF^2}{c_{KWM}} \frac{T}{T_0'} \tag{32}$$

with c_{KWM} the dimensionless celerity of Kinematic Wave model. Therefore, assuming an error less then 5%, Eq. (32) led Moramarco et al. (2008a) to deduce the following lower bound of wave duration:

$$\left.\frac{T}{T_0'}\right|_{5\%} = \frac{c_{KWM}}{KF^2}\Theta_{5\%} \tag{33}$$

in which the dimensionless celerity and the dimensionless wave period were set equal to $c^{TCW}_{KWM} = 3/2$ and $\Theta^{TCW}_{5\%} = 171$, respectively (Ponce et al., 1978).

As far as the power law fluids are concerned, Eq. (33) may be still applied provided that the dimensionless celerity c_{KWM} is evaluated through Eq. (13), i.e. $c_{KWM} = c^{PLF}_{KWM}$, and the dimensionless wave period threshold refers to the value deduced for power-law fluids $\Theta^{PLF}_{5\%}$ which depends on n as shown in Fig. 3b of Di Cristo et al. (2014). The $\Theta^{PLF}_{5\%}$

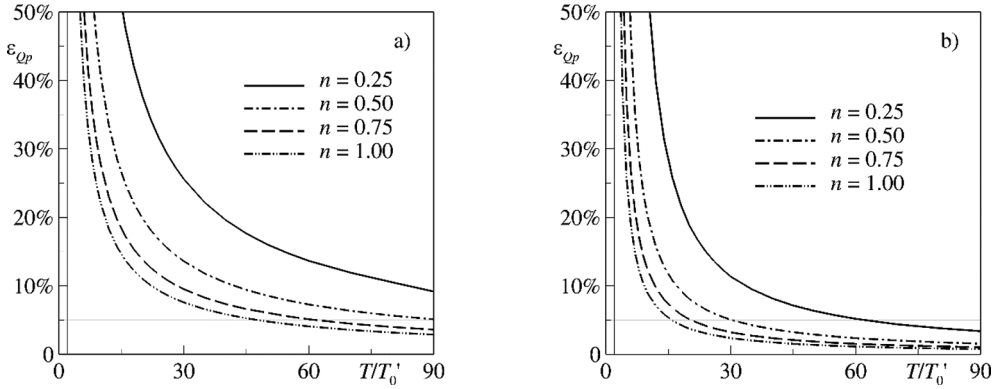

Fig. 5. Error of the peak discharge at the outlet ε_{Qp} as function of the ratio between the wave period and the wave reference travel time for different rheological indexes (n = 0.25, 0.50, 0.75, 1.0). F = 0.5. a) KF^2 = 2.5b) KF^2 = 20.

Table 2
Limiting stability Froude number and dimensionless wave period lower bounds from Di Cristo et al. (2014).

n	F^*	$\Theta_{5\%}^{PLF}$
0.25	0.20	90
0.50	0.35	102
0.75	0.47	92
1.0	0.58	91

values corresponding to the considered n values deduced from this figure are reported in Table 2.

The $T/T_0'|_{5\%}$ threshold given by Eq. (33) is depicted in Fig. 6 as function of KF^2, for the different n values assuming the values of $\Theta_{5\%}^{PLF}$ reported in Table 2. Therefore, accordingly to the wave period criterion, the KWM can be applied with an accuracy equal or larger than 95% in any of condition characterized by a (KF^2, T/T_0') pair laying above the theoretical curve.

Based on the results of the non-linear numerical simulations, for any of the conditions listed in Table 2 the value of T/T_0' above which the error of the three considered parameters is smaller than 5% is evaluated for several values of KF^2. In Fig. 6 triangles (circles) correspond to the mean error of the maximum depth (respectively discharge) $\varepsilon_{h\max}^*(\varepsilon_{q\max}^*)$, whereas squares represent the 5% error threshold value for the peak discharge ε_{Qp}. Void and filled symbols refer to the cases $F/F^* = 0.5$ and $F/F^* = 0.8$, respectively.

The ensemble of the results of the non-linear simulations reveals that the minimum T/T_0' value for KWM applicability decreases with both KF^2 and n. Moreover, a higher T/T_0' threshold is almost always required to assure the prescribed accuracy based on the ε_{Qp} parameter compared with the other two error metrics. For a fixed rheology, no substantial differences are observed between the two investigated Froude numbers.

Fig. 6 shows also that, independently of the Froude number value, for $n > 0.25$ and $KF^2 < 20$ the lines representing the Di Cristo et al. (2014)'s criterion are above all points. This means that it may be safely applied for predict all the considered quantities since it is more restrictive than the one resulting from the non-linear simulations. Such a conclusion holds even in the $KF^2 = 20$ case and for both the averaged maximum flow depth and the flow rate but not for the peak discharge. The above results apply even for n greater than 0.5 with exception of the $KF^2 = 2.5 - F/F^* = 0.5$ case for which $\varepsilon_{h\max}^*$ is always higher than the prescribed accuracy (results not shown). The performances of the wave period criterion deteriorate for the lowest value of n. In fact, independently on the Froude number, in the $KF^2 = 2.5$ case the mean error of the maximum depth is always higher than the prescribed accuracy (results not shown). Same conclusion holds even in for $KF^2 = 20$ as far as the maximum discharge and the peak discharge quantities are concerned.

4.3. Discussion and final remarks

The interest in using the KWM model for reproducing mud flow propagation implies the crucial question about its applicability. From a practical point of view, it is important to understand in which conditions its results represent a good approximation of the Full Model. Based on the presented study, the users interested in applying KWM to engineering problems involving mud flows are warned that its applicability range reduces as the rheological index decreases and it is significantly influenced by the KF^2 values. Moreover, as expected, the

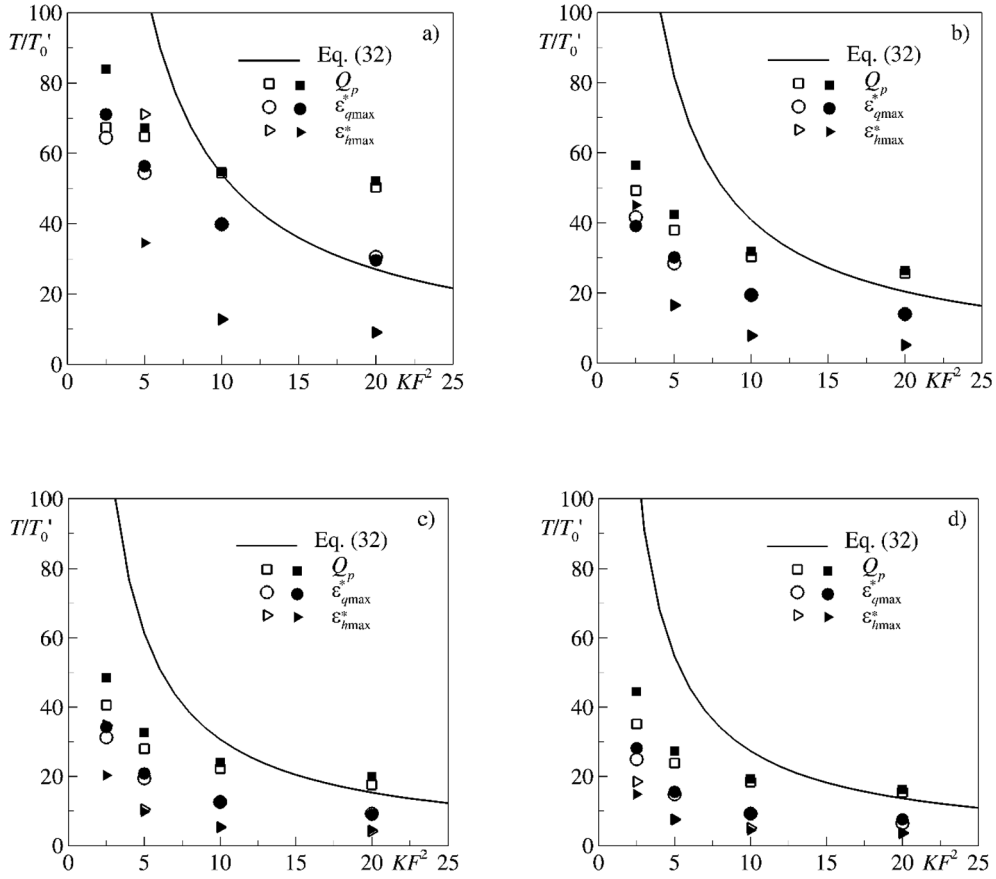

Fig. 6. . Minimum value of T/T_0' vs KF^2 corresponding to the mean error of the maximum flow depth $\varepsilon_{h\max}^*$ (triangle), the mean error of the maximum discharge $\varepsilon_{q\max}^*$ (circle) and the error of the peak discharge ε_{Qp} (square) is less than 5% as function of for $F/F^* = 0.5$ (void symbols) and $F/F^* = 0.8$ (filled symbols). Different values of rheological index: a). $n = 0.25$; b) $n = 0.50$; c) $n = 0.75$; d) $n = 1.0$. Continuous line: criterion by Di Cristo et al. (2014).

findings of the present analysis confirm that the KWM reproduces more reliable results for high values of the wave duration. The results indicate also that the applicability conditions depend on the flow variable of interest. The KWM reproduces with a better accuracy the maximum flow depth respect to the maximum flow discharge and the peak discharge at the outlet. In other words, complying with the applicability range relative to peak discharge guaranties the required accuracy also on both the maximum flow discharge and depth.

The study furnishes useful indications about the applicability condition of the KWM in terms of lower bound of dimensionless wave duration in order to have a mean error less than 5% on the reproduction of the considered flow variables. This parameter is equivalent to the dimensionless wave period adopted in the criteria used for clear-water (i.e. Ponce et al., 1978) and power-law fluids (i.e. Di Cristo et al., 2014).

The proposed criterion may be adopted to use KWM for simulating mud flow propagation in a channel after studying the fluid rheology and considering the hydrodynamic characteristics, i.e. F and K values. Based on it, according with the variable of interest, it is possible to define the minimum wave duration for which it may be adopted.

A further comparison demonstrated that, for power-law index values larger than 0.25, the wave period criterion obtained through a previous simpler linear analysis is more restrictive than the one deduced from the presented non-linear simulations, then it may be safely applied for all the considered variables.

The presented analysis has been carried out considering two Froude number values, namely $F = 0.5$ and $F = 0.8$. With reference to the Jiang-jia Ravine mud ($n = 0.3$, $\rho = 2130\,\mathrm{kg\,m^{-3}}$, $\mu = 150\mathrm{Pas^n}$, see Ng and Mei, 1994) and assuming a flow rate (for unit width) equal to $10\,\mathrm{m^2/s}$, the corresponding bottom slope is 0.3% and 0.5% for $F = 0.5$ and $F = 0.8$, respectively.

5. Conclusions

The present study investigates the applicability of the simplified Kinematic Wave Model (KWM) in predicting the unsteady propagation of a mud-flow wave, accounting for the non-linearity of the governing equations. The fluid, characterized by a highly-concentrated mixture of water and fine sediments, is represented through the power-law model proposed by Ng and Mei (1994). The analysis is performed through a numerical analysis of both the Full and Kinematic Wave models, adopting an explicit first-order scheme in time and a second-order Finite-Volume method for the spatial discretization. The applicability conditions are expressed considering three dimensionless indicators, related to the error on the maximum flow depth, the maximum discharge and the peak discharge at the downstream end of the channel.

The results indicate that the error on the maximum flow depth $\varepsilon_{h\max}$ increases moving in the downstream direction and that higher errors pertain to lower wave durations. The rheology substantially affects the magnitude of the errors which have been found to increase with the shear-thinning behavior of the fluid, i.e. to decrease with the rheological exponent n.

The analysis defines also the range of applicability of the KWM in terms lower bound of the wave duration T/T_0' above which the errors are within the 5%. The limiting value of T/T_0' depends on the rheological index and the dimensionless parameters F and KF^2, F and K being the Froude and the Kinematic wave numbers, respectively. The results indicate an increase of the T/T_0' lower bound (a reduction of the applicability range) as n decreases and a larger influence on it of KF^2 respect to F. The range of conditions in which the KWM has a mean error of the maximum flow depth less than 5% is wider than the one necessary for obtaining the same accuracy in terms of maximum flow discharge and peak discharge at the outlet.

Finally, the obtained criteria are compared with the wave period criterion theoretically deduced by Di Cristo et al. (2014) through a linear analysis. At least for moderate values of the dimensionless number KF^2 and for power law index values larger than 0.25, the wave period criterion has been found to be more restrictive than the one resulting from the non-linear analysis, which may be therefore safely adopted to assess the applicability of the Kinematic Wave Model to mud routing.

Declaration of Competing Interest

None.

Acknowledgement

The work described in the present paper was realized in the framework of the project MISALVA, financed by the Italian Minister of the Environment, Land Protection and Sea CUP H36C18000970005.

References

Ancey, C., 2007. Plasticity and geophysical flows: a review. J. Nonnewton. Fluid Mech. 142, 4–35. https://doi.org/10.1016/j.jnnfm.2006.05.005.
Arattano, M., Savage, W.Z., 1994. Modelling debris flows as kinematic waves. Bull. Int. Assoc. Eng. Geol. 49 (1), 3–13.
Arattano, M., Franzi, L., Marchi, L., 2006. Influence of rheology on debris-flow simulation. Nat. Hazards Earth Syst. Sci. 6, 519–528.
Aricò, C., Filianoti, P., Sinagra, M., Tucciarelli, T., 2016. The FLO diffusive 1D–2D model for simulation of river flooding. Water 8 (200). https://doi.org/10.3390/w8050200.
Armanini, A., Fraccarollo, L., Rosatti, G., 2009. Two-dimensional simulation of debris flows in erodible channels. Comput. Geosci. 35 (5), 993–1006.
Armanini, A., Larcher, M., Nucci, E., Dumbser, M., 2014. Submerged granular channel flows driven by gravity. Adv. Water Resour. 63, 1–10.
Bernard, M., Boreggio, M., Degetto, M., Gregoretti, C., 2019. Model-based approach for design and performance evaluation of works controlling stony debris flow with an application to a case study at Rovina di Cancia (Venetian Dolomites, Northeast Italy). Sci. Total Environ. 688, 1373–1388. https://doi.org/10.1016/j.scitotenv.2019.05.468.
Chanson, H., Jarny, S., Coussot, P., 2006. Dam Break Wave of Thixotropic Fluid. J. Hydraul. Eng. 132 (3), 280–293. https://doi.org/10.1061/(asce)0733-9429(2006)132:3(280).
Carotenuto, C., Merola, M.C., Ãlvarez-Romero, M., Coppola, E., Minale, M., 2015. Rheology of natural slurries involved in a rapid mudflow with different soil organic carbon content. Colloids Surf. A 466, 57–65. https://doi.org/10.1016/j.colsurfa.2014.10.037.
Chambon, G., Ghemmour, A., Laigle, D., 2009. Gravity-driven surges of a viscoplastic fluid: an experimental study. J. Nonnewton. Fluid Mech. 158, 54–62. https://doi.org/10.1016/j.jnnfm.2008.08.006.
Chambon, G., Ghemmour, A., Naaim, M., 2014. Experimental investigation of viscoplastic free-surface flows in a steady uniform regime. J. Fluid Mech. 754, 332–364. https://doi.org/10.1017/jfm.2014.378.
Chen, J.C., Jan, C.D., Lee, M.S., 2008. Reliability analysis of design discharge for mountainous gully flow. J. Hydraul. Res. 46, 835–838.
Chen, M., Liu, X., Wang, X., Zao, T., Zhou, J., 2019. Contribution of excessive supply of solid material to a runoff-generated debris flow during its routing along a gully and its impact on the downstream village with blockage effects. Water 11, 169. https://doi.org/10.3390/w11010169.
Chiang, S.H., Chang, K.T., Mondini, A.C., Tsai, B.W., Chen, C.Y., 2012. Simulation of event-based landslides and debris flows at watershed level. Geomorphology 138, 306–318. https://doi.org/10.1016/j.geomorph.2011.09.016.
Coussot, P., 1997. Mudflow Rheology and Dynamics. IAHR Monograph Series. Balkema, Rotterdam.
Deangeli, C., 2008. Laboratory granular flows generated by slope failures. Rock Mech. Rock Eng. 41 (1), 199–217. https://doi.org/10.1007/s00603-007-0131-1.
Di, B.F., Chen, N.S., Cui, P., Li, Z.L., He, Y.P., Gao, Y.C., 2008. GIS-based risk analysis of debris flow: an application in Sichuan, southwest China. Int. J. Sedim. Res. 23 (2), 138–148.
Di Cristo, C., Iervolino, M., Vacca, A., 2013a. On the applicability of minimum channel length criterion for roll waves in mud flows. J. Hydrol. Hydromech. 61 (4), 286–292. https://doi.org/10.2478/johh-2013-0036.
Di Cristo, C., Iervolino, M., Vacca, A., 2013b. Gravity-driven flow of a shear-thinning power-law fluid over a permeable plane. Appl. Math. Sci. 7 (33–36), 1623–1641. https://doi.org/10.12988/ams.2013.13150.
Di Cristo, C., Iervolino, M., Vacca, A., 2014. Simplified wave models applicability to shallow mud flows modeled as power-law fluids. J. Mt. Sci. 19, 956–965. https://doi.org/10.1007/s11629-014-3065-6.
Di Cristo, C., Evangelista, S., Iervolino, M., Greco, M., Leopardi, A., Vacca, A., 2018a. Dam-break waves over an erodible embankment: experiments and simulations. J. Hydraul. Res. 56 (2), 196–210. https://doi.org/10.1080/00221686.2017.1313322.
Di Cristo, C., Greco, M., Iervolino, M., Leopardi, A., Vacca, A., 2016. Two-dimensional two-phase depth-integrated model for transients over mobile bed. J. Hydraul. Eng. 142 (2), 04015043. https://doi.org/10.1061/(ASCE)HY.1943-7900.0001024.
Di Cristo, C., Iervolino, M., Vacca, A., 2017. A strategy for passive control of natural roll-waves in power-law fluids through inlet boundary conditions. J. Appl. Fluid Mech. 10

(2), 667–680. https://doi.org/10.18869/acadpub.jafm.73.238.26945.
Di Cristo, C., Iervolino, M., Vacca, A., 2018c. Applicability of kinematic and diffusive models for mud flows: a steady state analysis. J. Hydrol. 559, 585–595. https://doi.org/10.1016/j.jhydrol.2018.02.016.
Di Cristo, C., Iervolino, M., Vacca, A., 2018b. Wave propagation in linearized shallow flows of power-law fluids. Adv. Water Resour. 120, 35–49. https://doi.org/10.1016/j.advwatres.2017.06.022.
Dottori, F., Martina, M.L.V., Todini, E., 2009. A dynamic rating curve approach to indirect discharge measurement. Hydrol. Earth Syst. Sci. 13, 847–863.
Fernández-Nieto, E.D., Noble, P., Vila, J.P., 2010. Shallow water equations for non-Newtonian fluids. J. Nonnewton. Fluid Mech. 165 (13–14), 712–732. https://doi.org/10.1016/j.jnnfm.2010.03.008.
Fent, I., Putti, M., Gregoretti, C., Lanzoni, S., 2018. Modeling shallow water flows on general terrains. Adv. Water Resour. 12, 316–332. https://doi.org/10.1016/j.advwatres.2017.12.017.
Fenton, J., 2019. Flood routing methods. J. Hydrol. 570, 251–264.
Fuchs, S., Heiss, K., Hübl, J., 2007. Towards an empirical vulnerability function for use in debris flow risk assessment. Nat. Hazards Earth Syst. Sci. 7, 495–506.
Greco, M., Di Cristo, C., Iervolino, M., Vacca, A., 2019. Numerical simulation of mud-flows impacting structures. J. Mt. Sci. 16, 364–382. https://doi.org/10.1007/s11629-018-5279-5.
Gottlieb, S., Shu, C.W., 1998. Total variation diminishing Runge-Kutta schemes. Math. Comput. 67 (221), 73–85.
Govindaraju, R.S., Jones, S.E., Kavvas, M.L., 1988a. On the diffusion wave model for overland flow: solution for steep slopes. Water Resour. Res. 24 (5), 734–744. https://doi.org/10.1029/WR024i005p00734.
Govindaraju, R.S., Jones, S.E., Kavvas, M.L., 1988b. On the diffusion wave model for overland flow: steady state analysis. Water Resour. Res. 24 (5), 745–754. https://doi.org/10.1029/WR024i005p00745.
Gregoretti, C., Degetto, M., Boreggio, M., 2016. GIS-based cell model for simulating debris flow runout on a fan. J. Hydrol. 534, 326–340. https://doi.org/10.1016/j.jhydrol.2015.12.054.
Gregoretti, C., Degetto, M., Bernard, M., Boreggio, M., 2018. The debris flow occurred at Ru Secco Creek, Venetian Dolomites, on 4 August 2015: analysis of the phenomenon, its characteristics and reproduction by models. Front. Earth Sci. 6, 80. https://doi.org/10.3389/feart.2018.00080.
Gregoretti, C., Stancanelli, L.M., Bernard, M., Boreggio, M., Degetto, M., Lanzoni, S., 2019. Relevance of erosion process when modelling in-channel gravel debris flows for efficient hazard assessment. J. Hydrol. 568, 575–591. https://doi.org/10.1016/j.jhydrol.2018.10.001.
Harms-Ringdahl, L., 2004. Relationships between accident investigations, risk analysis, and safety management. J. Hazard. Mater. 111, 13–19.
Harten, A., Lax, P.D., van Leer, B., 1983. On upstream differencing and Godunov-type schemes for hyperbolic conservation laws. SIAM Rev. 25 (1), 35–61. https://doi.org/10.1137/1025002.
He, Y.P., Xie, H., Zhang, D.L., Cui, P., Wei, F.Q., Gardner, J.S., 2003. GIS-based hazard mapping and zoning of debris flow in Xiaojiang Basin, southwestern China. Environ. Geol. 45, 286–1283.
He, S., Liu, W., Ouyang, C., Li, X., 2014. A two-phase model for numerical simulation of debris flow. Nat. Hazard Earth Syst. Sci. 2, 2151–2183. https://doi.org/10.5194/nhessd-2-2151-2014.
Honda, N., Egashira, S., 1997. Prediction of debris flow characteristics in mountain torrents. In: Proceedings of the First International ASCE Conference on Debris-Flow Hazard Mitigation: Mechanics, Prediction and Assessment, San Francisco, CA, August 7–9, pp. 707–716.
Huang, X., Garcia, M.H., 1998. A Herschel-Bulkley model for mud flow down a slope. J. Fluid Mech. 374, 305–333. https://doi.org/10.1017/S0022112098002845.
Hwang, C.C., Chen, J.L., Wang, J.S., Lin, J.S., 1994. Linear stability of power law liquid film flowing down an inclined plane. J. Phys. D: Appl. Phys. 27, 2297–2301. https://doi.org/10.1088/0022-3727/27/11/008.
Hungr, O., 2011. quantitative analysis of debris torrent hazard for design of remedial measures. Can. Geotech. J. 21 (4), 663–677.
Hurlimann, M., Copons, R., Altimir, J., 2006. detailed debris flow hazard assessment in Andorra: a multidisciplinary approach. Geomorphology 78, 359–372.
Iverson, R.M., George, D.L., 2014. A depth-averaged debris-flow model that includes the effect of evolving dilatancy. I Physical basis. Proc. R. Soc. A Math. Phys. Eng. Sci. 470, 1–31. https://doi.org/10.1098/rspa.2013.0819.
Jacob, M., Stein, D., Ulmi, D., 2012. Vulnerability of buildings to debris flow impact. Nat. Hazards 60 (2), 241–261. https://doi.org/10.1007/s11069-011-0007-2.
Jeong, S.W., Leroueil, S., Locat, J., 2009. Applicability of power law for describing the rheology of soils of different origin and characteristics. Can. Geotech. J. 46, 1011–1023.
Longo, S., Di Federico, V., Chiapponi, L., 2015. Non-Newtonian power-law gravity currents propagating in confining boundaries. Environ. Fluid Mech. 15, 515. https://doi.org/10.1007/s10652-014-9369-9.
Longo, S., Chiapponi, L., Di Federico, V., 2016. On the propagation of viscous gravity currents of non-Newtonian fluids in channels with varying cross section and inclination. J. Nonnewton. Fluid Mech. 235, 95–108. https://doi.org/10.1016/j.jnnfm.2016.07.007.
Medina, V., Hurlimann, M., Bateman, A., 2008. Application of FLATModel, a 2D a finite volume code to debris flows in the northeastern part of the Iberian Peninsula. Landslide 5, 127–142. https://doi.org/10.1007/s10346-007-0102-3.
Mei, C.C., Liu, K.F., Yuhi, M., 2001. Mud flow— slow and fast. In: Balmforth, N.J., Provenzale, A. (Eds.), Geomorphological Fluid Mechanics. Lecture Notes in Physics. Springer, Berlin, Heidelberg.
Moramarco, T., Pandolfo, C., Singh, V.P., 2008a. Accuracy of kinematic wave and diffusion wave approximations for flood routing. I: steady analysis. J. Hydrol. Eng. 13 (11), 1078–1088. https://doi.org/10.1061/(ASCE)1084-0699(2008)13:11(1078).
Moramarco, T., Pandolfo, C., Singh, V.P., 2008b. Accuracy of Kinematic Wave approximations for flood routing. II: unsteady analysis. J. Hydrol. Eng. 13 (11), 1089–1096. https://doi.org/10.1061/(ASCE)1084-0699(2008)13:11(1089).
Moussa, R., Boequillon, C., 1996. Criteria for the choice of flood routing methods in natural channels. J. Hydrol. 186, 1–30. https://doi.org/10.1016/S0022-1694(96)03045-4.
Ng, C., Mei, C.C., 1994. Roll waves on a shallow layer of mud modeled as a power-law fluid. J. Fluid Mech. 263, 151–184. https://doi.org/10.1017/S0022112094004064.
Noble, P., Vila, J.P., 2013. Thin power-law film flow down an inclined plane: consistent shallow-water models and stability under large-scale perturbations. J. Fluid Mech. 735, 29–60. https://doi.org/10.1017/jfm.2013.454.
O'Brien, J.S., Julien, P.Y., Fullerton, W.T., 1993. Two-dimensional water flood and mudflow simulation. J. Hydraul. Eng. 119 (2), 244–261. https://doi.org/10.1061/(ASCE)0733-9429(1993) 119:2(244).
Ovarlez, G., Mahaut, G., Bertrand, F., Chateau, X., 2011. Flows and heterogeneities with a vane tool: magnetic resonance imaging measurements. J. Rheol. 55 (2), 197–223.
Pastor, M., Blanc, T., Haddad, B., Petrone, S., Sanchez Morles, M., Drempetic, V., Issler, D., Crosta, G.B., Cascini, L., Sorbino, G., Cuomo, S., 2014. Application of a SPH depth-integrated model to landslide run-out analysis. Landslides 11, 793–812. https://doi.org/10.1007/s10346-014-0484-y.
Perazzo, C.A., Gratton, J., 2004. Steady and traveling flows of a power–law liquid over an incline. J. Nonnewton Fluid Mech. 118, 57–64. https://doi.org/10.1016/j.jnnfm.2004.02.003.
Perumal, M., Sahoo, B., 2007. Applicability criteria of the parameter Muskingum stage and discharge routing methods. Water Resour. Res. 43 (5), W05409. https://doi.org/10.1029/2006WR004909.
Perumal, M., Moramarco, T., Sahoo, B., Barbetta, S., 2007. A methodology for discharge estimation and rating curve development at ungauged river sites. Water Resour. Res. 43, 2 0043-1397/07/2005WR004609.
Pitman, E.B., Le, L., 2005. A two-fluid model for avalanche and debris flows. Philos. Trans. R. Soc. A 363, 1573–1601. https://doi.org/10.1098/rsta.2005.1596.
Ponce, V.M., Li, R.M., Simons, D.B., 1978. Applicability of kinematic and diffusion models. J. Hydraul. Div. 104 (HY3), 353–360.
Pudasaini, S.P., 2011. Some exact solutions for debris and avalanche flows. Phys. Fluids 23, 043301. https://doi.org/10.1063/1.3570532.
Pudasaini, S.P., 2012. A general two-phase debris flow model. J. Geophys. Res. 117, F03010. https://doi.org/10.1029/2011JF002186.
Ruyer-Quil, C., Manneville, 2002. Further accuracy and convergence results on the modeling of flows down inclined planes by weighted-residual approximations. Phys. Fluids 14 (1), 170–183. https://doi.org/10.1063/1.1426103.
Rosatti, G., Begnudelli, L., 2013. Two dimensional simulations of debris flows over mobile beds: enhancing the TRENT2D model by using a well-balanced generalized Roe-type solver. Comput. Fluids 71, 179–185. https://doi.org/10.1016/j.compfluid2012.10.006.
Singh, V.P., Aravamuthan, Y., 1996. Errors of kinematic-wave and diffusion-wave approximations for steady-state overland flows. CATENA 27 (3–4), 209–227. https://doi.org/10.1016/0341-8162(96)00021-5.
Stancanelli, L.M., Musumeci, R.E., 2018. Geometrical characterization of sediment deposits at the confluence of mountain streams. Water 10 (4), 401. https://doi.org/10.3390/w1004040.
Takahashi, T., 1991. Debris flows. IAHR Monograph. Balkema, Rotter-dam.
Takahashi, T., 2014. Debris Flows: Mechanics, Prediction and Countermeasures. Taylor and Francis, Balkema, Leiden.
Thiene, M., Shaw, W.D., Scarp, R., 2017. Perceived risks of mountain landslides in Italy: stated choices for subjective risk reductions. Landslide 14, 1077–1089. https://doi.org/10.1007/s10346-016-0741-3.
Tsai, C.W., 2003. Applicability of kinematic, noninertia, and quasisteady dynamic wave models to unsteady flow routing. J. Hydraul. Eng. 129 (8), 613–627. https://doi.org/10.1061/(ASCE)0733-9429(2003) 129:8(613).
Toro, E., 2009. Riemann Solvers and Numerical Methods for Fluid Dynamics. Springer, Berlin.
VanDine, D.F., 1985. Debris flow and debris torrents in the Southern Canadian Cordillera. Can. Geotech. J. 22, 44–68.
Weill, S., Chiara-Roupert, R., Ackerer, P., 2014. Accuracy and deficiency of time integration methods for 1D diffusive wave equation. Comput. Geosci. 18, 697–709. https://doi.org/10.1007/s10596-014-9417-z.
Yan, K., Di Baldassarre, G., Solomatine, D.P., 2013. Exploring the potential of SRTM topographic data for flood inundation modelling under uncertainty. J. Hydroinf. 15, 849–861.
Yu, D., Lane, N., 2006. Urban fluvial flood modelling using a two-dimensional diffusion-wave treatment, part 1: mesh resolution effect. Hydrol. Process. 20, 1541–1565. https://doi.org/10.1002/hyp.5935.
Zhang, X., Bai, Y., Ng, C.O., 2010. Rheological properties of some marine muds dredged from china coasts. In: Proceedings of the 28 International Offshore and Polar Engineering Conference, pp. 455–461.
Zucco, G., Tayfur, G., Moramarco, T., 2015. Reverse flood routing in natural channels using genetic algorithm. Water Resour. Manage. 29 (12), 4241–4267.